Energy & Environmental Science

ROYAL SOCIETY OF CHEMISTRY

PAPER

View Article Online
View Journal | View Issue

Cite this: *Energy Environ. Sci.*, 2023, **16**, 4650

Decarbonising electrical grids using photovoltaics with enhanced capacity factors†

Cai Williams,[a] Hannes Michaels,[b] Andrew F. Crossland,[c] Zongtai Zhang,[a] Natasha Shirshova,[a] Roderick C. I. MacKenzie,[a] Hongjian Sun,[a] Jeff Kettle,[d] Marina Freitag[b] and Christopher Groves*[a]

Received 27th February 2023,
Accepted 7th September 2023

DOI: 10.1039/d3ee00633f

rsc.li/ees

Many scenarios for Net Zero anticipate substantial growth of Solar PV generation to satisfy 30% of our electricity needs. However, this scale of deployment introduces challenges as supply may not meet demand, thereby necessitating energy storage and demand-side management. Here we demonstrate a different, complementary approach to resolving this challenge in which Solar PV generation can be made intrinsically less variable than commercial PV. Proof-of-concept dye-sensetised PVs for which the power conversion efficiency increases as light intensity reduces are demonstrated. Modelling of the UK mainland energy network predicts that these devices are more effective at displacing high carbon generation from coal and gas than commercial PV. The capacity factor of these PV devices are controlled by their design, and capacity factors >60% greater than silicon are predicted based on experimental data. These data demonstrate a new approach to designing PV devices in which minimising variability in generation is the goal. This new design target can be realised in a range of emerging technologies, including Perovskite PV and Organic PV, and is predicted to be more effective at delivering carbon reductions for a given energy network than commercial PV.

Broader context

Achieving Net Zero requires substantial expansion of clean renewable energy generation as well as methods to account for variable generation which may overlap poorly with demand. Thus, it is expected that energy storage and management of demand will be needed alongside Solar PV which generates energy in proportion to the strength of sunlight. In this paper we demonstrate a new, complementary solar PV technology where generation can be made more efficient at lower light levels, thereby introducing flexibility in energy generation that is intrinsically absent in present Solar PV. Using this approach, we demonstrate that the new PV devices are more effective at displacing high-carbon generation from coal or gas at the national scale than present solar PV technology. This represents a new approach to solar PV, in which the goal is minimising variability in generation, and with it, the need for energy storage and demand side management.

Introduction

Commercial Photovoltaic (PV) technology based on silicon is technologically mature, deployable at scale,[1,2] and currently one of the cheapest renewable sources of energy.[3] For these reasons, roadmaps to achieve Net Zero anticipate PV will grow from 3% of global electricity generation[4] to over 20% in the next few decades.[4–6] However, the shift from dispatchable (*i.e.* can be turned on as needed) to variable renewable generation including significant contributions from PV creates a range of challenges. From a carbon perspective, time-resolved PV generation does not match demand in many areas of the world, which in turn may necessitate the use of dispatchable fuels like gas, coal, biomass, hydrogen or synthetic fuels to meet the shortfall. Variable renewable generation also creates difficulties for electricity system operators (ESOs), which must meet demand near instantaneously whilst maintaining the supplied voltage and frequency within certain limits, *i.e.* provide a defined ''power quality''. For example, in some markets such as California, maintaining power quality is a particular challenge around sunset when generation swings from Solar PV to dispatchable sources rapidly over a short space of time, and the

[a] *Department of Engineering, Durham University, South Road, Durham, DH1 3LE, UK. E-mail: chris.groves@durham.ac.uk*
[b] *Department of Chemistry, Bedson Building, Newcastle University, Newcastle upon Tyne, NE1 7RU, UK*
[c] *Durham Energy Institute, Durham University, South Road, Durham, DH1 3LE, UK*
[d] *James Watt School of Engineering, University of Glasgow, Glasgow, Scotland, UK*
† Electronic supplementary information (ESI) available. See DOI: https://doi.org/10.1039/d3ee00633f

magnitude of this swing increases with Solar PV penetration (the so-called ''Duck Curve'' effect[7]). Power quality is also an issue for low voltage networks, such as those on which most rooftop solar panels are connected, since reverse power flow during sunny periods can lead to overvoltage.[8,9] Commercial PV also faces financial challenges as it is predicted that revenues will reduce as PV penetration increases,[10–12] though it is noted this may not be true for all energy markets. This value deflation has led some to advocate for more ambitious cost targets for silicon PV to ensure they remain cost competitive.[12] All these issues have their root in the relative lack of control as to when PV generates power and are expected to become more serious as the penetration of PV increases. It is expected that grid-level energy storage[13] and demand-side management[14] will play a key role in mitigating these challenges, however, the roll-out of these technologies is arguably not keeping pace with the installation of Solar PV. This motivates the question: can the variability in PV generation itself be minimised?

In the electrical power industry, variability of renewable generation is quantified by the capacity factor, which is the ratio of the actual energy output to the theoretical maximum energy output over a set period. Capacity factors for commercial silicon PVs vary with the local climate, for example, ranging from 10% in the UK[15] to over 25% in California.[16] Generally, the capacity factors offered by silicon PV do not compare favourably with other forms of energy generation, for example, the UK's National Statistics Agency estimated in 2021[15] that Offshore wind had a capacity factor of 38%, whilst Biomass had 64%, and Nuclear had 59% (though we note that this is a low value for Nuclear from a historical perspective). Maximising capacity factor through generator design is a recognised approach in the wind power sector[17] to address the challenges of variable generation listed above.[18] However, at present, the techniques to increase capacity factor in solar PV are limited and external to the solar cell itself, such as installation of east/west facing panels to extend generation into the morning and evening,[19,20] or the use of tracking mounts.[21,22]

In this paper we demonstrate a class of PV devices that have intrinsically higher capacity factor than conventional PV technology. These devices, which we term High Capacity Factor Photovoltaics, or CFPV, have a power conversion efficiency (PCE) which increases as irradiance reduces. This behaviour boosts generation at times of low irradiance to both minimise variability in power output and maximise power harvested for a given capacity of grid connection. The benefits that CFPV devices offer for matching supply and demand are demonstrated using a model of the mainland UK energy network. In this context, it is shown that CFPV generation matches demand more effectively than an equivalent capacity of silicon PV, and that this leads to two key benefits that increase with capacity factor: (i) a reduced need for high carbon intensity generation from coal or gas, and (ii) increased income from wholesale markets. CFPV devices based on a dye-sensitised architecture are demonstrated, showing that the capacity factor can be controlled through rational design. Further, the improvement in capacity factor through device design is predicted to be larger than available with external methods, such as single- and dual-axis tracking. Introducing control of the generation profile of Solar PV in this way is expected to reduce the need for, and costs associated with, energy storage and demand-side management elsewhere in the wider energy system.

Results and discussion

Our approach in this work was to use energy systems modelling to establish the benefits of CFPV devices on national carbon emissions and income generation, and demonstrate that CFPV behaviour can be designed rationally through PV device structure. In other words, we aimed to demonstrate both a 'demand pull' (*i.e.* benefits of CFPV) and a 'technology push' (*i.e.* ability to design CFPV behaviour) to motivate future work in this area. This paper is organised to discuss the benefits of CFPV at the grid scale first, before moving on to report results from designed CFPV devices.

Modelling CFPV generation at the national scale

To establish the benefits of CFPV, we required both a model of a CFPV device and of an energy network. Considering first the model of the CFPV device, it has been shown that Organic,[23–27] Perovskite[28–31] and Dye-Cell[32,33] PV architectures can have increasing PCE with reducing light intensity, which may in turn give rise to CFPV behaviour. We selected from these papers[23–33] the data reported by Bristow and Kettle[33] shown in Fig. 1, for a commercial (SolarPrint, Dublin), large-area (5×5 cm) dye-sensitised PV module measured in an outdoor test (Bangor, Wales). Here slow ion transportation in the electrolyte led to limited mass transport under high irradiance and lower PCE. Thus, lowering irradiance from 1000 Wm^{-2} reduced the required transportation rate and increased the PCE. We stress that our selection of the devices from Bristow and Kettle[33] was due to the measurements being taken outdoors on a large-area PV device to provide a realistic test

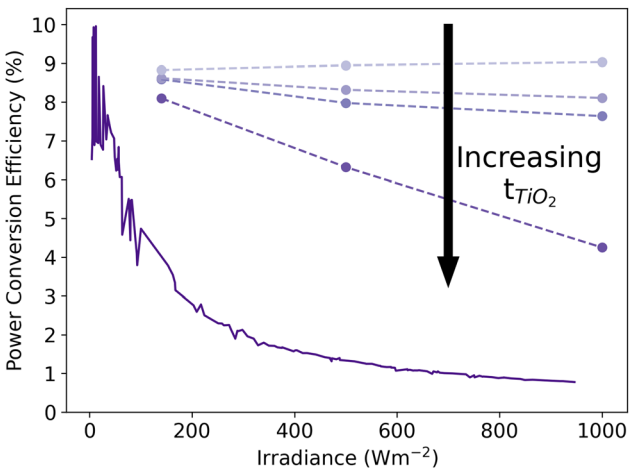

Fig. 1 PCE irradiance characteristics of CFPV devices as reported by[33] (line), and those devices reported here (symbols) with t_{TiO_2} = 12 (pentagons), 18 (squares), 24 (triangles) and 48 μm (circles).

of the CFPV concept. Other PVs based on Perovskite[28–31] or Organic[23–27] absorbers have also been shown to achieve CFPV behaviour as well as different PCE under AM1.5 conditions. The opportunities this raises for future CFPV technologies will be discussed in the context of the results later in the paper.

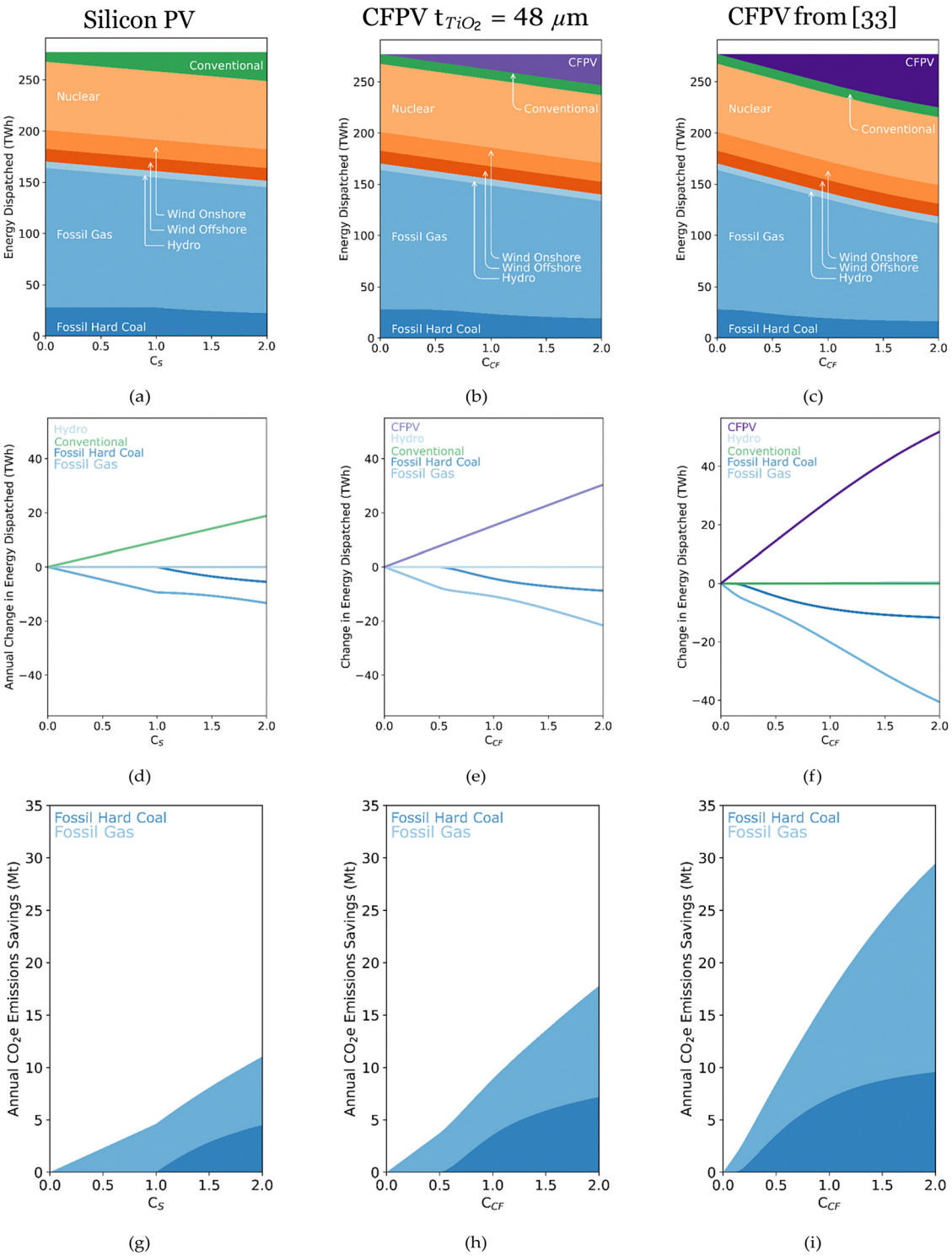

Fig. 2 Annual generation profiles of the UK (a)–(c), change in generation (d)–(f) and carbon savings (g)–(i) as a function of additional silicon PV (a), (d), (g), and CFPV for t_{TiO_2} = 48 μm devices shown in Fig. 1b (b), (e), (h) and CFPV device[33] (c), (f) and (i). Change in generation (d), (e) and (f) figures show change in generation against 2016 historical data. Carbon savings (g), (h) and (i) figures show the source of carbon savings from reduction in Gas (Light Blue) and Coal (Dark Blue) emissions.

To quantify how the behaviour shown in Fig. 1 may impact national generation profiles and consequent carbon emissions, a plant dispatch model of the mainland UK electrical network (inc. England, Wales, and Scotland) was developed to predict and compare carbon savings that result from adding varying amounts of CFPV or silicon PV. The mainland UK was selected as the location for our analysis due to the good availability of generation data, as well as having a mismatch between irradiance (which peaks at midday) and electricity demand (which peaks in the late afternoon) as is common for national and large-scale electricity networks including Brazil, California, Chile, India, Iran, Spain and South Africa to name a few.[34–36] The UK receives lower irradiance than many countries in the world due to its northerly latitude, however, we stress that increasing the capacity factor of solar PV also has value in sunnier locations. For example, tracking improves capacity factor, and in 2021 more than 85% of US deployed utility scale solar PV capacity (*i.e.* solar farms of more than 5 MW) incorporated some aspect of tracking.[37] These tracking systems were installed in high-irradiance states such as California, Arizona and Texas, as well as less sunny mid-western states, showing there is an economic advantage in increasing capacity factor in both low- and high-irradiance locations.

With the location selected, energy supply within the plant dispatch model was divided into differing dispatch classes (DCs), which represent technologies that are similar in terms of their ability to be curtailed and carbon intensity. These are: DC1, which includes nuclear; DC2 which includes hydrogeneration, curtailable utility scale PV and Wind; DC3 which represents energy storage; whilst DC4 is carbon-intensive gas and coal. The capacities of each DC are listed in ESI† Table S1. Time-resolved energy demand for the year 2016 was assumed to be the sum of dispatched energy for each half-hourly time period,[11] and this demand was met within the model with energy from increasing dispatch classes within each time window, whilst integrating the associated carbon intensity. A flow chart of the dispatch process is shown in ESI† Fig. S1, and a table of the carbon intensity for varying forms of generation is shown in ESI† Table S1. The plant dispatch model was modified from that of Crossland *et al.*[12] to incorporate PV generation with arbitrary PCE-irradiance characteristics. A detailed description of the calculations and the use of these data is included in ESI† Section S2, but is summarized briefly here. PV generation in DC2 was modelled at a half-hourly resolution using insolation and generation data from the photovoltaic geographical information system[38] (PVGIS) and balancing mechanism reporting service[39] (BMRS). The power generation capability of silicon PVs in the model is based on real historical data, thus we did not specify a PCE-irradiance characteristic. Conversely, for CFPV, we scaled the generation for silicon PV in each time window by an enhancement factor, E derived from the measured PCE irradiance characteristics for CFPV devices:

$$E(l) = \frac{\mathrm{PCE}(l)}{\mathrm{PCE}(1000)} \quad (1)$$

where l is the irradiance in the specified time window, and PCE(1000) is the PCE measured at 1000 Wm^{-2}. This approach ignores differences in temperature coefficients between silicon PV and CFPV devices.

We highlight that the data related to UK energy mix (*e.g.* Fig. 2) will be reported in terms of energy dispatched, *i.e.* where the energy was drawn from when it was used to satisfy demand, as opposed energy generated. In most cases, energy generated was dispatched immediately (ESI† Table S1 and Fig. 2a–c), in which case dispatch and generation are synonymous. However, excess generation can also be used to charge energy storage that can be used later, decoupling when energy is generated and when it is dispatched. As an illustrative example, excess solar generation which charges storage which is later dispatched to satisfy demand would be counted as coming from storage rather than solar. Counting energy in this way enabled us to examine how changes in generation alters the usage of energy storage. Fig. S1 of the ESI† describes the process of charging storage in more detail.

We took as our reference the mainland UK electrical grid with associated generation and storage assets in the year 2016, which included 11 970 $\mathrm{MW_P}$ installed PV that was dominated by silicon, and added to this an additional capacity of silicon PVs (C_{Si}) or CFPVs (C_{CF}). The values of C reported here are expressed as a fraction of installed UK PV capacity in 2016 (11 970 $\mathrm{MW_P}$) which defined the power generating capability when irradiance was 1000 Wm^{-2}. Thus, a simulation for $C_{\mathrm{CF}} = 0.5$ assumes an additional capacity of CFPV assets equal to 50% of the UK PV capacity in DC2 in 2016. We frame our discussion in terms of installed capacity as it is this quantity that significantly affects connections of renewable energy to the grid, including procedure, duration and cost of grid connections.[40] In other words, the substations and wires where the solar farm connects to the wider network have a defined capacity, meaning that the solar farm must operate safely on the network without causing any other issues, such as reduced power quality and loss of network protection.[40] Further detail as to how the network limits the scope of distributed generation in the UK context is available from the Energy Networks Association in both summary[41] and detailed form.[42]

Benefits of CFPV behaviour on national carbon emissions

The CFPV behaviour shown in Fig. 1 was input to the plant dispatch model. Our discussion initially focuses on comparing model predictions for conventional silicon PV and the CFPV devices reported by Bristow and Kettle.[33] Fig. 2a and c show the predicted annual UK mix of dispatched energy as a function of additional PV capacity for silicon PV and CFPV devices respectively. Fig. 2d and f shows the same information in as Fig. 2a and c respectively, but expressed as a change in annual dispatched energy. For both silicon and CFPV, additional generation from solar reduced the need for carbon intensive generation from coal and gas, as well as improving the utilisation of hydropower due to the increased opportunity to 'charge' reservoirs during periods of energy surplus. More importantly, these data show that CFPV devices are more effective per installed capacity at reducing fossil fuel usage than silicon PV.

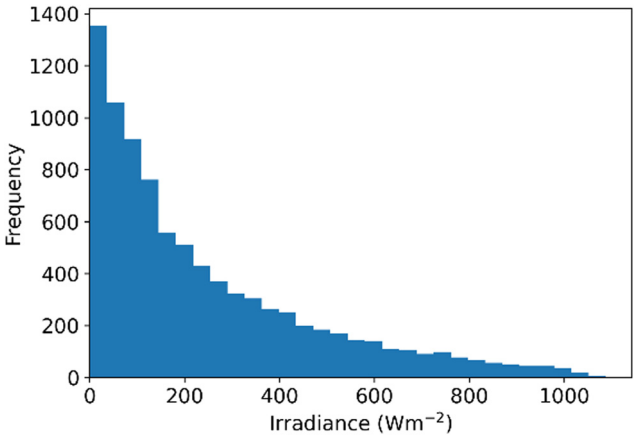

Fig. 3 Histogram of irradiance in the UK during July as an example of data used in calculations.

This effectiveness in decarbonization can be quantified by the annual Carbon Dioxide equivalent (CO_2e) emissions calculated by the plant dispatch model. Fig. 2g and i show predicted CO_2e emissions savings as generation capacity was increased for both silicon PV and CFPV respectively. As expected, CO_2e savings increased with generation capacity for both PV technologies, however, we observed the rate at which this occurs is non-linear as it becomes progressively more difficult to satisfy demand that does not align to irradiance. These data revealed that the CFPV device is approximately twice as effective at decarbonizing the grid for an equivalent amount of silicon PV over the range of C examined. Hence grid-scale CFPV was predicted to be more successful in reducing Carbon emissions than the equivalent capacity of installed silicon PV. When one reflects on the scale of PV installation that has been forecast to achieve Net Zero at the national level,[4–6] and the consequent PV market penetration this implies, we argue that these data make a strong case for CFPV to be part of the energy generation mix to address some of the inflexibility that silicon PV has in meeting 'hard to decarbonize' energy demand.

The reason for the greater impact of CFPV as compared to silicon PV was its superior yield at irradiances below 1000 Wm^{-2}. Fig. 3 shows a histogram of the irradiance values used in the model corresponding to July. Diurnal variation and weather results in a mean irradiance during daylight hours of 259 Wm^{-2}, for which the CFPV device reported by Bristow and Kettle[33] had a PCE enhancement of factor E(259 Wm^{-2}) = 2.94 as compared to standard testing conditions (Fig. 1). Thus, the CFPV device was providing a power output in real conditions that was closer to its rated capacity than the silicon equivalent.

Enhanced capacity factors for PV

The beneficial behaviour of the CFPV device in the previous section can be quantified by the capacity factor, which as a reminder, is the ratio of the actual energy generated over a period to the theoretical maximum energy generated over the same period. Model predictions of the capacity factor for devices considered here are shown in Table 1. Typically the capacity factor of solar installations varies between 10% and 25% depending on the level of insolation.[11] In the UK where we based our analysis, the temperate climate and high latitude results in PV capacity factors of around 10%,[15] which agrees well with present model predictions for silicon PV of 8.89%. The CFPV device reported by Bristow and Kettle,[33] by contrast, is predicted to have a capacity factor of 27.40% in the UK, more than 3 times larger than silicon PV.

Benefits of CFPV behaviour on income generation on wholesale markets

As with Carbon emissions, the real-time balance between supply and demand is also critical in determining revenues from PV generation assets. If generation from different grid-connected PV farms is aligned in time, as occurs in climatically similar regions such as California for example, an over-supply of solar energy depresses the wholesale price of energy, particularly if the fraction of PV generation capacity is large (>10%).[10–12] Conversely, if demand is not met from renewables then the wholesale price of energy climbs, representing an unmet need that may be met by high carbon intensity generation. To demonstrate the possibilities of revenue generation from CFPV, we estimated the annual income from a 5 MW_P solar farm and compared it to that expected from silicon PV. Our rationale for this approach is that a 5 MW_P solar farm would be large enough to sell electricity on the wholesale market but not so large as to significantly perturb the market price. In the calculations, we accumulated revenue in each settlement period over the course of a year and ignored the possibility of penalties for under- and over-generation,[43] and assumed that the PV installation makes no change to the

Table 1 Experimental data related to CFPV devices as well as predicted CO_2e savings for C = 1, capacity factor, and wholesale earnings and costs for a 5 MW_P solar farm. Methodologies for prediction of these numbers are included in the ESI as described in the main text

Device	PCE at 1000 Wm^{-2} (%)	PCE (140 Wm^{-2})/ PCE (1000 Wm^{-2})	Annual CO_2e savings when C = 1 (Mt)	Predicted UK capacity factor (%)	Predicted wholesale revenue for 5 MW_P farm sited in UK (k€)	Predicted module costs (€/W_P)
Conventional Si PV	20	0.9	4.70	8.89	194	0.245
CFPV, t_{TiO_2} = 12 μm	9.0	1.00	4.61	8.87	191	0.355
CFPV, t_{TiO_2} = 18 μm	8.1	1.06	5.00	9.36	201	0.395
CFPV, t_{TiO_2} = 24 μm	7.6	1.10	5.28	9.67	209	0.420
CFPV, t_{TiO_2} = 48 μm	4.3	1.90	9.00	14.50	315	0.740
SolarPrint CFPV reported in 33	0.8	5.20	17.00	27.40	611	4.000

marginal cost of energy. A full description of the calculations is provided in Section S3 of the ESI.†

The silicon solar farm was estimated to yield €194 000 over the year, whilst an equal capacity installation of CFPVs with characteristics reported by Bristow and Kettle[33] was estimated to yield €611 000, more than 3 times as much. This additional income is due to increased generation when irradiance is below 1000 Wm^{-2}, which in a UK context, is a large proportion of the time (see *e.g.* Fig. 3). However, the greater income that the CFPV device provides should be viewed in the context of lower efficiencies under standard testing conditions (PCE = 0.8% under AM1.5), since this would be expected to lead to greater module costs (particularly deriving from the TCO[44]) and land costs for the same generating capacity. To quantify this anticipated trade-off, we used the approach described in ESI† Section S3 to estimate the cost of commercially produced dye-sensitised CFPVs of the type described by Bristow and Kettle[33] at 28.54 €m^{-2}, and in turn, predicted the module cost per unit capacity (€/W_P) shown in Table 1. These module costs were predicted to increase with reducing PCE under standard testing conditions, with CFPV modules from ref. 33 costing 16 times more than the Silicon equivalent. Allied to this, land rent costs also increased as PCE under standard testing conditions reduced, as shown in ESI† Table S3, though land rent costs are predicted to be smaller than that of the modules themselves for a 5 MW_P solar farm.

Hence, for CFPV modules with characteristics as reported by Bristow and Kettle,[33] we have demonstrated an intrinsic increase in capacity factor and thus more efficient utilisation of a grid connection, but that the low PCE at AM1.5 in this case leads to substantial increases in module and land costs. We now move on to discuss the second aspect of our investigation, namely to ascertain whether the CFPV behaviour of devices can be designed. Were this to be the case, CFPV devices could be designed to balance the characteristic behaviours highlighted for the Bristow and Kettle[33] device.

Device fabrication and measurements

We selected a dye-sensitised architecture shown in Fig. 4 as a candidate CFPV due to its high efficiency in low light conditions.[45] The basic design of the present CFPVs followed that of Saygili *et al.*, namely comprising the organic Y123 dye and the copper(II/I) bis(4,4′,6,6′-tetramethyl-2,2′-bipyridine) bis(trifluoromethanesulfonyl)imide (known as Cu(tmby)$_2$) electrolyte.[46] The cells were assembled with poly(3,4-ethylenedioxythiophene) counter electrodes, allowing the photoanode to be in direct contact with the cathode.[47] The devices were assembled based on two-layered titania photoanodes, comprising an initial layer of photoactive 30 nm nanoparticles with thicknesses of t_{TiO_2} = 12, 18, 24 and 48 μm, each capped by a 6 μm scattering layer consisting of 400 nm TiO_2 nanoparticles acting as a back reflector. At low light intensities, the effective diffusion length of ions in the electrolyte can be assumed to be the total TiO_2 thickness to first approximation as the counter electrode attaches directly behind the scattering layer. Thus, by changing t_{TiO_2} the diffusion length of ions in the electrolyte can be controlled.

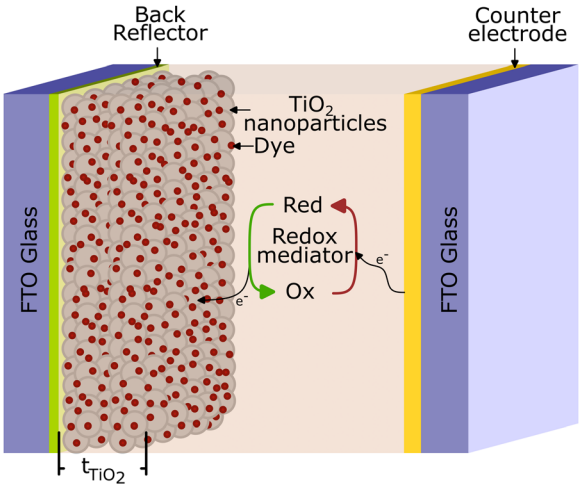

Fig. 4 Schematic for present devices in which TiO_2 thickness was varied over the range t_{TiO_2} = 12, 18, 24, 48 μm.

Fig. 1 shows PCE as a function of irradiance for CFPV devices with varying t_{TiO_2}. PCE was largely constant with irradiance for the device with small t_{TiO_2} (= 12 μm), and thus has similar PCE-irradiance behaviour as commercial silicon,[48] albeit with a lower efficiency. As t_{TiO_2} increased beyond 12 μm, it was observed that PCE reduced. Importantly in the context of this paper, the reduction in PCE depended on irradiance, with PCE under high irradiance reducing more than under low irradiance. We ascribed this reduction to the photocurrent generation of dye-sensitised PVs being limited by diffusion mass transport,[49] which in turn reduced performance to an extent that depends upon both t_{TiO_2} and irradiance. Critically, we demonstrated that the PCE-irradiance behaviour for these devices was controlled by the PV layer stack.

Energy systems modelling utilising designed CFPV devices

Fig. 1 shows that the PCE – irradiance characteristic for the present devices form a series with the Bristow and Kettle device.[33] As t_{TiO_2} is increased from 12 μm to 48 μm, the PCE at 1000 Wm^{-2} is reduced, whilst the PCE at low intensity is largely unchanged. The device reported by Bristow and Kettle device[33] is an extreme version of the t_{TiO_2} = 48 μm device, with even lower efficiency at 1000 Wm^{-2}.

Model predictions for the designed CPFV devices are summarised in Table 1. The devices with t_{TiO_2} = 12 μm, 18 μm and 24 μm, for which there is limited increase in PCE as irradiance reduces (E(140 Wm^{-2}) ≤ 1.1), show limited improvements in capacity factor, decarbonisation and revenue generation. These data are shown in more detail in ESI† Fig. S2 and S3.

These data contrast to that for the t_{TiO_2} = 48 μm device, for which the PCE increased by a factor of E(140 Wm^{-2}) = 1.9 (Table 1), which in turn translated to a more substantial modification of generation and associated benefits. Focusing on capacity factor in particular, the device with t_{TiO_2} = 12 μm had a capacity factor of 8.87%, which compared to 14.5% for

t_{TiO_2} = 48 μm, more than 60% larger. This enhancement in PV capacity factor by device design is larger than for both single-axis (~10–35%) and dual-axis (~30–45%) tracking systems[50,51] and does not require mechanical tracking systems. Looking in more detail at these data, Fig. 2b, e and h show predicted annual generation mix, change in energy dispatch, and CO_2e savings respectively as capacity of t_{TiO_2} = 48 μm CFPV devices is increased. It can be seen that even for the modest value of E(140 Wm^{-2}) = 1.9 given by this device results in up to 60% improvement in carbon savings compared to the silicon equivalent. These data emphasise that the benefits associated with CFPV are due to an increase in PCE with reducing light intensity, and not the absolute value of PCE at low irradiance.

We now turn to examine the costs associated with the designed CFPV devices. As it is the PCE under 1000 Wm^{-2} that determines the rated power of a solar installation, an increase in PCE under these conditions will lead to a reduction in cost. Thus, the predicted module costs for the designed CFPV devices are all substantially lower than for the Bristow and Kettle[33] CFPV device which has lower PCE. Focusing on the t_{TiO_2} = 48 μm CFPV device, the predicted module cost is only 3 times higher than the silicon equivalent, contrasting with 16 times higher for the Bristow and Kettle[33] CFPV device.

These data have thus shown that changing t_{TiO_2} thickness offers control over both CFPV benefits and module cost. However, this was realised by controlling efficiency at AM1.5 (Fig. 1), such that there was a trade-off between costs (related to PCE at AM1.5) and enhanced capacity factor (related to increase in PCE with reducing light intensity). As such, changing t_{TiO_2} thickness alone did not realise low costs and enhanced capacity factor simultaneously. That said, we highlight that cost is not the only consideration from a system perspective, as electricity supply operators must ensure reliable power supply from a diverse range of sources to meet demand when faced with varying generation from renewables. For example, Nuclear is an important part of the energy mix in the UK despite its high levelised cost of energy because of the reliable base load it provides.[52] Thus, more expensive and less variable solar generation may still represent value from a system perspective.

Nonetheless, the costs of the designed CFPV devices motivates us to consider how one may achieve low costs and CFPV benefits simultaneously. In ESI† Section S4, we present data for Dye Cells engineered to give high capacity factor behaviour by another route, namely by changing electrolyte concentration. These data show that we again control the PCE *vs.* irradiance characteristics through device design, but again this is through a reduction in PCE at AM1.5, in a similar fashion to Fig. 1. Notwithstanding this, we expect that there is still opportunity for small improvement in costs associated with dye-sensitised CFPVs as the present record efficiency for a dye-sensitised PV device under AM1.5 conditions is 13.5%,[53] which is higher than the 10% achieved for the t_{TiO_2} = 12 μm device here.

We suggest that the larger opportunity may be in the creation of CFPV devices with Organic[23–27] or Perovskite[28–31] absorber layers, as higher PCEs in these devices can mitigate costs whilst still realising the benefits of increasing PCE as light

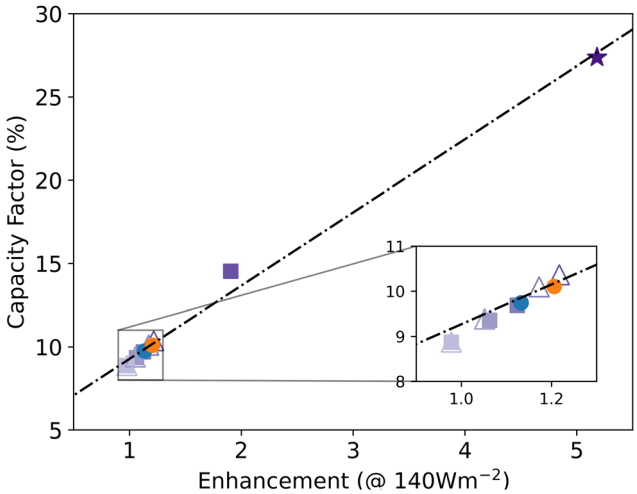

Fig. 5 Predicted UK capacity factor for PV devices considered in this study as a function of enhancement factor at 140 Wm^{-2}. Purple closed squares: dye-cell CFPV with t_{TiO_2} from 12 μm (light) to 48 μm (dark, purple) – Table 1; purple open triangles: dye-cell CFPV with Cu_M^{2+} from 0 M (light) to 0.06 M (dark) – ESI† Fig. S6; purple closed star – Bristow and Kettle dye-cell PV[33]; blue filled circle – Du *et al.* Perovskite PV;[28] orange filled circle – Nam *et al.* organic PV.[23]

intensity reduces. To demonstrate this opportunity, we repeated the above plant dispatch analysis using data for a quarternary Organic PV device reported by Nam *et al.*,[23] and a MAPI Perovskite PV device from Du *et al.*,[28] both of which display CFPV behaviour. Fig. 5 shows the predicted capacity factor for these devices as a function of enhancement factor at l = 140 Wm^{-2} alongside all other devices considered in this paper. It is observed that the predicted capacity factor varies approximately linearly with enhancement factor for all device types, showing the generality of the approach. We highlight that the enhancement factor is accessible in lab experiments, offering a straightforward first-order method to assess suitability of candidate PVs for CFPV applications. More detailed assessments of suitability would require measurement of the PCE-irradiance characteristic and analysis using the available code. Finally, while the capacity factors for the Perovskite and Organic PV device are modest compared to the Dye-Cell devices developed here, we recall that these devices were not designed for CFPV applications and so optimisation is likely to yield improvements.

Conclusions

In this paper we have introduced the concept of High Capacity Factor PV where the variation in output power is minimised by engineering PCE to increase as irradiance decreases. Energy systems modelling at a national level demonstrate that CFPVs of this type are more effective in reducing carbon emissions than a similar capacity of silicon PVs due to the reduced need for high carbon-intensity generation, and subsequently greater revenue potential as supply better meets demand. We also show experimental data for Dye-Cell based CFPVs in which the PCE

vs. irradiance characteristic is controlled, which in turn is shown to tune the cost, carbon abatement and capacity factor offered by the technology. We believe that this approach presents an alternative, complementary approach to decarbonising electrical grids, as rather than relying solely on energy storage and demand management to account for inflexible, intermittent renewable generation, one incorporates flexibility in the generation itself. Further, we highlight literature reports which suggest that Perovskite and Organic PVs can also be used realise the high capacity factor concept, opening up the possibility of new applications for emerging PV technologies.

Experimental procedures

Fabrication of photovoltaic cells

The dye-sensitised solar cells were fabricated according to Michaels *et al.*[54] On cleaned (RBS solution, water, ethanol, UV-ozone) Nippon sheet glass (Pilkington, St. Helens, UK), 10 Ω sheet resistance, a dense TiO_2 layer was deposited *via* spray pyrolysis at 450 °C from a 0.2 M titanium bis(isopropoxide) bis(acetylacetonate) solution in isopropanol.[55] Subsequently, 0.384 cm^2 (7 mm diameter circles) TiO_2 photoanodes were screen-printed (Seritec Services SA, Corseaux, Switzerland) from DSL 30 NRD-T (Dyesol/GreatCellSolar, Queanbeyan, Australia) colloidal (30 nm) TiO_2 paste (4 μm). After brief drying at 120 °C, a scattering layer (Dyesol/GreatCellSolar WER2-0, 400 nm) was screen-printed onto of the mesoporous film (4 μm), followed by gradual heating towards a 30 minute sintering step at 500 °C. The substrates were post-treated with a 13 mM aqueous $TiCl_4$ solution for 30 min at 70 °C and then sintered again at 450 °C for 30 min. After cooling, the titania films were immersed into the sensitiser solution consisting of 0.1 mM Y123 dye (Dyenamo, Stockholm, Sweden) and 0.2 mM chenodeoxycholic acid (Sigma) in acetonitrile 1 : 1 *tert*-butanol for 16 hours. PEDOT counter electrodes were manufactured *via* electropolymerization of 3,4-ethylenedioxythiophene (Sigma) from a 0.01 mM aqueous solution with 0.1 M sodium dodecyl sulphate.[56] The redox electrolyte solutions for the DSCs were prepared with 0.2 M $Cu(tmby)_2TFSI$ and 0.04 M $Cu(tmby)_2TFSI_2$ (both from Dyenamo), 0.1 M lithium bis(trifluoromethanesulfonyl) imide (Sigma) and 0.6 M *N*-methyl benzimidazole in acetonitrile. All cells were assembled using ThreeBond (Düsseldorf, Germany) 3035B UV glue and cured with a CS2010 UV-source (Thorlabs, Newton, NJ, USA). The electrolyte was injected through a hole in the counter electrode, which was then sealed with additional UV glue.

Characterization of photovoltaic cells

Current–voltage measurements under AM 1.5G illumination were carried out in ambient air using a HelioSim-CL60 solar simulator (Voss electronic GmbH). The irradiation intensity was asserted with a certified reference diode (Fraunhofer). An X200 source meter (Ossila, Sheffield, UK) was used to assess the solar cell performance (scan speed 25 mV s^{-1}, 200 ms). A circular mask was employed to confine the active solar cell area to 0.196 cm^2. The shown efficiency trends with illumination level are averages of four to six cells at all times, pending reasonable error margins of the manual cell fabrication.

Data and code availability

Python codes embodying the Plant Dispatch model and Solar Farm cost calculations, as well as an Excel Worksheet for cost calculation of dye sensitised devices, are available from Durham Research Online **https://doi.org/10.15128/r2xs55mc10f**.

Author contributions

C. W. – software, validation, investigation, writing (original draft), writing (review and editing), visualisation. H. M. – investigation, writing (original draft), writing (review and editing). A. C. – software, validation, investigation, writing (review an editing). Z. Z. – software, validation. N. S. – supervision, writing (review and editing). R. M. – supervision, writing (review and editing). H. S. – validation, writing (review and editing). J. K. – investigation, writing (review and editing). M. F. – supervision, writing (review and editing), funding acquisition. C. G. – conceptualization, writing (original draft), writing (review and editing), project administration, funding acquisition.

Conflicts of interest

The authors declare no competing interests.

Acknowledgements

We gratefully acknowledge funding from the EPSRC Centre for Doctoral Training in Renewable Energy Northeast Universities (EP/S023836/1), and the North East Centre for Energy Materials (EP/R021503/1).

References

1 IEA. Renewable Energy Market Update. Report, 2020.
2 IEA. Solar PV Global Supply Chains. Report, 2022.
3 US Energy Information Administration. Levelised costs of New Generation Resources. Report, 2022.
4 IEA. Net Zero by 2050: A roadmap for the Global Energy Sector. Report, 2021.
5 IRENA. Future of solar photovoltaic: deployment, investment, technology, grid integration and socio economic aspects. Report, 2019.
6 Shell. ''Sky: Meeting to goals of the Paris Agreement'', 2018.
7 California ISO. What the duck curve tells us about managing a green grid. Report, 2016.
8 A. Kharrazi, V. Sreeram and Y. Mishra, Assessment techniques of the impact of grid-tied rooftop photovoltaic generation on the power quality of low voltage distribution network – A review, *Renewable Sustainable Energy Rev.*, 2020, **120**, 109643.

9 M. Karimi, *et al.*, Photovoltaic penetration issues and impacts in distribution network – A review, *Renewable Sustainable Energy Rev.*, 2016, **53**, 594–605.
10 D. Millstein, *et al.*, Solar and wind grid system value in the United States: The effect of transmission congestion, generation profiles, and curtailment, *Joule*, 2021, **57**, 1749–1775.
11 J. Chase, View from the Solar Industry: We Don't Need COP26 to Shine, But What Should We Worry About?, *Joule*, 2022, **6**(3), 495–497.
12 V. Sivaram and S. Kann, Solar power needs a more ambitious cost target, *Nat. Energy*, 2016, **14**, 16036.
13 IRENA. Electricity Storage and Renewables: Costs and Markets to 2030. Report. International Renewable Energy Agency, 2017.
14 IRENA. Demand Side Flexibility for Power Sector Transformation: Analytical Brief. Report. International Renewable Energy Agency, 2019.
15 National Statistics Digest of UK Energy Statistics (DUKES). Government Document, 2022.
16 US Energy Information Administration. Annual Electric Generator Inventory. Report, 2019.
17 E. J. Lantz*et al.*, IEA Wind TCP Task 26: Impacts of Wind Turbine Technology on the System Value of Wind in Europe. Report, 2017.
18 R. Wiser, *et al.*, The hidden value of large-rotor, tall-tower wind turbines in the United States, *Wind Eng.*, 2021, **454**, 857–871.
19 H. Wirth and K. Schneider. Recent facts about photovoltaics in Germany, Fraunhofer Ise, 2015, **92**.
20 D. Peper, S. Lange and C. Kost, *Photovoltaikzubau In Deutschland In Zahlen*, Fraunhofer ISE, 2019.
21 S. Abdallah, The effect of using sun tracking systems on the voltage–current characteristics and power generation of flat plate photovoltaics, *Energy Convers. Manage.*, 2004, **4511**, 1671–1679.
22 M. Bolinger and J. Seel. Utility Scale Solar: Empirical Trends in Project Technology, Cost, Performance and PPA pricing in the United states 2018. Report. Laurence Berkeley National Labo ratory, 2018.
23 M. Nam, *et al.*, Semi-transparent quaternary organic blends for advanced photovoltaic applications, *Nano Energy*, 2019, **58**, 652–659.
24 Kwon Y., *et al.*, Revealing conflicting effects of solvent additives on morphology and performance of non-fullerene organic photovoltaics under different illuminance conditions, *Dyes Pigm.*, 2022, **207**, 110754.
25 R. Munir, *et al.*, Air-processed organic photovoltaics for outdoor and indoor use based upon a tin oxide-perylene diimide electron transporting bilayer, *Adv. Mater. Interfaces*, 2022, **93**, 2101918.
26 X. Rodrıguez-Martınez, *et al.*, Matching electron transport layers with a non-halogenated and low synthetic complexity polymer: fullerene blend for efficient outdoor and indoor organic photovoltaics, *J. Mater. Chem. A*, 2022, **1019**, 10768–10779.
27 R. Steim, *et al.*, Organic photovoltaics for low light applications, *Solar Energy Mater. Solar Cells*, 2011, **95**, 3256–3261.
28 T. Du, *et al.*, Light-intensity and thickness dependent efficiency of planar perovskite solar cells: charge recombination versus extraction, *J. Mater. Chem. C*, 2020, **836**, 12648–12655.
29 Y. Reyna, *et al.*, Performance and stability of mixed $FAPbI_3$ (0.85) $MAPbBr_3$ (0.15) halide perovskite solar cells under outdoor conditions and the effect of low light irradiation, *Nano Energy*, 2016, **30**, 570–579.
30 V. Stoichkov, *et al.*, Outdoor performance monitoring of perovskite solar cell mini-modules: diurnal performance, observance of reversible degradation and variation with climatic performance, *Solar Energy*, 2018, **170**, 549–556.
31 J. Dagar, *et al.*, Highly efficient perovskite solar cells for light harvesting under indoor illumi- nation via solution processed SnO_2/MgO composite electron transport layers, *Nano Energy*, 2018, **49**, 290–299.
32 E. Tanaka, *et al.*, Synergy of co-sensitizers in a copper bipyridyl redox system for efficient and cost-effective dye-sensitized solar cells in solar and ambient light, *J. Mater. Chem. A*, 2020, **83**, 1279–1287.
33 N. Bristow and J. Kettle, Outdoor organic photovoltaic module characteristics: Benchmarking against other PV technologies for performance, calculation of Ross coefficient and outdoor stability monitoring, *Sol. Energy Mater. Sol. Cells*, 2018, **175**, 52–59.
34 IEA. ''Real-Time Electricity Tracker'', 2023. **https://www.iea.org/data-and-statistics/data-tools/real-time-electricity-tracker**.
35 California ISO. ''CAISO'', 2023. **https://www.caiso.com**.
36 Red Electrica. ''DEMANDA DE ENERGIA ELE CTRICA EN TIEMPO REAL'', 2023. **https://demanda.ree.es/visiona/home**.
37 M. Bolinger*et al.* Utility-Scale Solar, 2022 edition, Report, 2022.
38 T. Huld, R. Muller and A. Gambardella, A new solar radiation database for estimating PV performance in Europe and Africa, *Solar Energy*, 2012, **866**, 1803–1815.
39 Elexon. ''Balancing Mechanism Reporting Service (BMRS)'', 2022. **https://www.bmreports.com**.
40 Ricardo-AEA. Wales Energy Energy Toolkit: Grid Connection Module. Web Page, 2015.
41 Energy Networks Association (UK). Distributed Generation Connection Guide. Report, 2020.
42 Engineering Networks Association. Technical Requirements for Customers' Export and Import Limitation Schemes (Issue 2): G100 A1. Report, 2022.
43 Imbalance Pricing - BSC Guidance Notes - Elexon BSC. Web Page.
44 G. Hashmi, *et al.*, Review of materials and manufacturing options for large area flexible dye solar cells, *Renewable Sustainable Energy Rev.*, 2011, **158**, 3717–3732.
45 A. Belén Muñoz-García, *et al.*, Dye-sensitized solar cells strike back, *Chem. Soc. Rev.*, 2021, **5022**, 12450–12550.
46 Y. Saygili, *et al.*, Copper Bipyridyl Redox Mediators for Dye-Sensitized Solar Cells with High Photovoltage, *J. Am. Chem. Soc.*, 2016, **138**, 15087–15096.

47 Y. Cao, *et al.*, Direct Contact of Selective Charge Extraction Layers Enables High-Efficiency Molecular Photovoltaics, *Joule*, 2018, **26**, 1108–1117.
48 Product Specification - REC Twinpeak 4 Black Series. **https://www.recgroup.com/sites/default/files/documents/ds_rec_twinpeak_4_black_series_en.pdf?t=1663844604**.
49 R. García-Rodríguez, *et al.*, Improving the mass transport of copper-complex redox mediators in dye-sensitized solar cells by reducing the inter-electrode distance, *Phys. Chem. Chem. Phys.*, 2017, **19**, 32132–32142.
50 A. F. Almarshoud, Performance of solar resources in Saudi Arabia, *Renewable Sustainable Energy Rev.*, 2016, **66**, 694–701.
51 E. Drury, *et al.*, Relative performance of tracking versus fixed tilt photovoltaic systems in the USA, *Prog. Photovoltaics*, 2014, **22**, 1302–1315.
52 National Audit Office. Nuclear Power in the UK. Report. National Audit Office, 2016.
53 D. Zhang, *et al.*, A molecular photosensitizer achieves a V_{oc} of 1.24 V enabling highly efficient and stable dye-sensitized solar cells with copper(II/I)-based electrolyte, *Nat. Commun.*, 2021, **12**, 1777.
54 H. Michaels, *et al.*, Dye-sensitized solar cells under ambient light powering machine learning: towards autonomous smart sensors for the internet of things, *Chem. Sci.*, 2020, **11**, 2895–2906.
55 H. Michaels and M. Freitag, Assessment of TiO_2 Blocking Layers for CuII/I-Electrolyte Dye-Sensitized Solar Cells by Electrochemical Impedance Spectroscopy, *ACS Appl. Energy Mater.*, 2022, **52**, 1933–1941, DOI: **10.1021/acsaem.1c03433**.
56 H. Ellis, *et al.*, PEDOT Counter Electrodes for Dye-Sensitized Solar Cells Prepared by Aqueous Micellar Electrodeposition, *Electrochimica Acta*, 2013, **107**, 45–51.